IOPscience iopscience.iop.org

Home Search Collections Journals About Contact us My IOPscience

Statistics of resonances for a class of billiards on the Poincaré half-plane

This article has been downloaded from IOPscience. Please scroll down to see the full text article.

2005 J. Phys. A: Math. Gen. 38 10829

(http://iopscience.iop.org/0305-4470/38/49/022)

View the table of contents for this issue, or go to the journal homepage for more

Download details:
IP Address: 171.66.16.94
The article was downloaded on 03/06/2010 at 04:04

Please note that terms and conditions apply.

INSTITUTE OF PHYSICS PUBLISHING JOURNAL OF PHYSICS A: MATHEMATICAL AND GENERAL

J. Phys. A: Math. Gen. **38** (2005) 10829–10841 doi:10.1088/0305-4470/38/49/022

Statistics of resonances for a class of billiards on the Poincaré half-plane

P J Howard[1], **F Mota-Furtado**[1], **P F O'Mahony**[1] **and V Uski**[1,2]

[1] Department of Mathematics, Royal Holloway, University of London, Egham, Surrey TW20 0EX, UK
[2] Department of Physics, University of Turku, 20014 Turku, Finland

E-mail: p.j.howard@rhul.ac.uk

Received 5 July 2005, in final form 12 October 2005
Published 22 November 2005
Online at stacks.iop.org/JPhysA/38/10829

Abstract

The lower boundary of Artin's billiard on the Poincaré half-plane is continuously deformed to generate a class of billiards with classical dynamics varying from fully integrable to completely chaotic. The quantum scattering problem in these open billiards is described and the statistics of both real and imaginary parts of the resonant momenta are investigated. The evolution of the resonance positions is followed as the boundary is varied which leads to large changes in their distribution. The transition to arithmetic chaos in Artin's billiard, which is responsible for the Poissonian level-spacing statistics of the bound states in the continuum (cusp forms) at the same time as the formation of a set of resonances all with width $\frac{1}{4}$ and real parts determined by the zeros of Riemann's zeta function, is closely examined. Regimes are found which obey the universal predictions of random matrix theory (RMT) as well as exhibiting non-universal long-range correlations. The Brody parameter is used to describe the transitions between different regimes.

PACS numbers: 05.45.Mt, 03.65.Nk

1. Introduction

The quantum mechanics of billiard systems on surfaces of negative curvature has been extensively studied over the last two decades, since the discovery that some compact billiards on those surfaces had spectral statistics which violated the famous conjecture of Bohigas–Giannoni–Schmit [1, 2] relating the level-spacing statistics to those of the Gaussian ensembles for different symmetry groups. See [3] for an early review and introduction to the classical and quantum descriptions of this geometry. Explanations for these phenomena have since been forthcoming and the term 'arithmetic chaos' [4] coined to categorize them, since they are due to those particular symmetries of the groups whose fundamental domains coincide with the

billiards. Whereas a lot of work has been done on the bound states for such systems, much less is known about the resonances in the continuum. Here, for the first time to the authors' knowledge, an analysis is presented of the resonance spectrum for a whole class of hyperbolic billiards which includes Artin's billiard.

The simplest arithmetic group is the modular group, and Artin's billiard corresponds to half the fundamental domain of that group. It thus shares one symmetry class of eigenfunctions and eigenvalues of the Laplacian defined on the full domain. It has also been considered as a model for the early universe in [5] and, extended to three dimensions, in [6]. Deformations to the domain, including a fully-integrable case, were studied in [5] for the case of Dirichlet boundary conditions on the billiard walls. Here, we consider the same class of deformations, but for the billiard with von Neumann boundary conditions on all walls. This difference changes the nature of the quantum system fundamentally, for it allows states which escape to infinity, thus opening the system and putting us in the realm of scattering theory.

Remarkably, the scattering theory for the special case of Artin's billiard is analytically solvable and of particular interest due to the resonances being determined by the non-trivial zeros of Riemann's zeta function [7]. These are well known to possess Gaussian unitary ensemble (GUE) level-spacing statistics [8]. It is also the case for Artin's billiard that a set of bound states exist superimposed on the scattering continuum (so-called 'cusp forms' in mathematics). Such states arise in atomic scattering when the parameters of a system conspire to give zero coupling to the continuum, and are extremely sensitive to perturbation of those parameters [10]. Here the cusp forms are treated as part of the resonance continuum. The variation of the resonance positions on smoothly changing the boundary of the billiard is studied. For the statistics of the real parts of the resonance positions, one sees in the nearest-neighbour distribution the transition from Poissonian for the integrable case to Gaussian orthogonal ensemble (GOE) and back to Poissonian again in the arithmetic case. For the width distribution, it is shown how it evolves into a χ^2 distribution initially, but then splits into two distinct groups, one of which moves closer to the real axis and the other which forms the resonances given by the zeros of the Riemann zeta function. As the boundary is further varied, the χ^2 distribution is again recovered. The two-point correlation function is also studied through the Fourier transforms of the spectra and the correlation between the positions and widths is examined. Both universal correlations predicted by RMT and non-universal correlations are found in certain parameter ranges.

The billiard system and deformation considered are introduced in section 2 as well as the methods involved in the calculation of the resonances. The statistics of the resonances are investigated in section 3 and conclusions are reserved for section 4.

2. Billiards on the Poincaré half-plane

Artin's billiard is the infinite triangle in the Poincaré half-plane representation of hyperbolic geometry with angles $\pi/2$, $\pi/3$ and 0. This is the triangle bounded by the unit circle and the lines $x = 1/2$ and $x = 0$, or using a complex plane notation it is the right-hand half of the modular domain, defined by the lines $z = \pm 1/2 + iy$ and the inequality $|z| \geqslant 1$.

In the scheme of Csordás *et al* [5], the lower boundary of the domain is parameterized by a real number, the 'control parameter' $0 \leqslant C_p \leqslant 2$. C_p is the inverse radius of the circle passing through $z = \imath$ which has its centre on the imaginary axis in $\mathrm{Im}(z) \leqslant 0$. Thus, on the lower boundary

$$y = 1 - \frac{C_p x^2}{1 + \sqrt{1 - C_p^2 x^2}}. \tag{1}$$

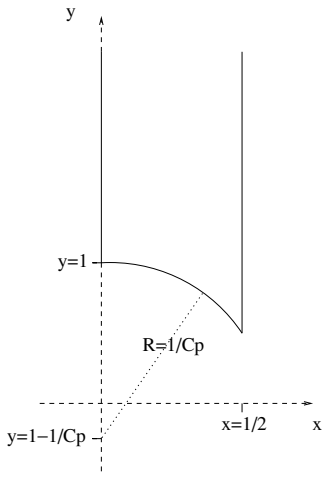

Figure 1. The billiards considered on the Poincaré half-plane.

The integrable case corresponds to $C_p = 0$, i.e. the boundary lies at $y = 1$, and Artin's billiard has $C_p = 1$. For $C_p > 2$, the lower part of the billiard becomes open as well as the top. Here, the variation of the resonance spectrum is studied as C_p varies continuously in the range $0 < C_p \leqslant 2$.

Since the metric in the Poincaré half-plane is $g_{ij} = y^{-2}\delta_{ij}$, the appropriate Schrödinger equation for these billiards is

$$y^2\left(\frac{\partial^2}{\partial x^2} + \frac{\partial^2}{\partial y^2}\right)\Psi = -\lambda\Psi, \tag{2}$$

where $\lambda = 2mE/\hbar^2 + \frac{1}{4}$ and E is the energy of a particle of mass m [7, 11].

Solutions of (2) are sought which obey von Neumann boundary conditions on all walls. Considering first this boundary condition on $x = 0$ and $x = 1/2$, that is

$$\frac{\partial\Psi}{\partial\hat{n}} = 0, \tag{3}$$

where $\frac{\partial}{\partial\hat{n}}$ is the normal derivative of the wavefunction on the boundary, one can separate (2) and write an infinite set of solutions which obey (3) for fixed λ that decay (as y tends to infinity), in the form

$$\psi_m(k; x, y) = \cos(2\pi mx)\sqrt{y}K_{\imath k}(2\pi my), \quad m \in \mathbb{N}, \tag{4}$$

where $k = \sqrt{2mE}/\hbar$ is the scaled momentum and $K_{\imath k}$ is the modified Bessel function of imaginary order.

The above solutions together with the continuum solution of the form

$$\psi_0(k; y) = y^{1/2}(y^{-\imath k} + S(k)y^{\imath k}), \tag{5}$$

which represents incoming and outgoing waves at infinity, form a complete set of states for the scattering problem. S is the scattering matrix, here a scalar since there is only one scattering channel possible. To satisfy the boundary condition (3) on the lower boundary in figure 1 at an arbitrary energy E one must take a linear combination of the above solutions in (4) and (5).

In order to calculate the resonance energies, one must enforce the outgoing wave boundary condition at infinity instead of the form given in (5), i.e. we replace (5) by $\psi_0(k; x, y) = y^{1/2+\imath k}$. The full wavefunction is thus expanded in the form

$$\Psi_N(k; x, y) = \sum_{m=0}^{N-1} A_m \psi_m(k; x, y). \tag{6}$$

This wavefunction by construction represents a resonance state and obeys the von Neumann boundary condition at $x = 0$ and $x = 1/2$. Finally to determine the coefficients A_m and the complex resonance eigenenergies or eigenmomenta k, one must enforce the von Neumann boundary condition on the lower boundary. To do this one uses a modified collocation method, following the example of Csordás *et al* [5] (see [13] for further discussion of the method's advantages). One calculates the normal derivative of (6) on the lower boundary and Fourier expands it into a set of N orthogonal functions $\sin\left(\frac{n\pi s}{L}\right)$.

The Fourier coefficients of this expansion D_n are given by

$$D_n = \sum_{m=0}^{N-1} C_{nm} A_m, \tag{7}$$

where

$$C_{nm} = \oint \mathrm{d}s \sin\left(\frac{n\pi s}{L}\right) \frac{\partial \psi_m}{\partial \hat{n}}(k; s), \qquad n = 1, \ldots, N. \tag{8}$$

s is a parametrization of the lower billiard boundary and L its length in that parametrization. Here, the simple relation

$$s = x \tag{9}$$

is taken on the lower boundary, where the normal derivative is given by

$$\frac{\partial}{\partial \hat{n}} = y\left(C_p x \frac{\partial}{\partial x} + \sqrt{1 - C_p^2 x^2}\frac{\partial}{\partial y}\right) \tag{10}$$

in this parameterization and x ranges from 0 to $L = 1/2$. The normal derivative is identically zero on the rest of the boundary by construction. The boundary condition on the lower boundary is now satisfied by setting the Fourier coefficients equal to zero or equivalently by searching for the complex values k such that the determinant of the $N \times N$ complex matrix C_{nm} is zero. The summations are necessarily truncated at N, but N is chosen sufficiently large to achieve convergence of the eigenvalues. The higher the energy of the resonance the more values of n and m are required. A scaling with momentum of $N = \mathrm{int}(r_{\mathrm{scal}} + 1)$, where $r_{\mathrm{scal}} = 3\,\mathrm{Re}(k)/4\pi$ and int means taking the integer part of the expression, was found to yield zeros to the desired precision compared with the known cases $C_p = 0$ and $C_p = 1$. For higher values of N, the Bessel functions included become exponentially small and do not contribute significantly.

After scaling each row of the matrix by its largest element to avoid overflowing the maximum computational precision available, a singular-value decomposition is performed to ease detection of the complex zeros [14, 15]. The method produces results in agreement with those in the literature [16, 17, 9] for the known case of $C_p = 1$ and with separately calculated values for $C_p = 0$, to the desired precision.

In the integrable case ($C_p = 0$), the scattering has no resonances. All the eigenvalues are real and are given by the zeros of the derivatives at $y = 1$ of the functions (4) given above, that is they are determined by the condition

$$\left[\frac{\partial}{\partial y}(\sqrt{y} K_{\imath k}(2\pi m y))\right]_{y=1} = 0. \tag{11}$$

These corresponding eigenvalues, k_n, were calculated using Mathematica's [18] FindRoot function.

In order to calculate the widths and positions of the resonances at new values of C_p, first many eigenvalues for the integrable problem ($C_p = 0$) were calculated as described above. Using these values as seeds for the calculation, C_p is varied a little, and a search in the complex plane for zeros of the least singular value of the matrix $\boldsymbol{C}$ near to the old values is performed. Then C_p can be varied again, by larger amounts at each step, as information about the velocity of each resonance with C_p allows better guesses as to the perturbed value.

The most time consuming part of the routine aside from the iterations required to reach any desired value of C_p is the setting up of the matrix (8) due to the many calculations of the Bessel functions (here involving complex values of k) required for each element. Powerful expansions similar to those in [5] are used taken mostly from [19] but largely based on routines used in [20].

The second case where there are results available [16, 17, 9] to check against those obtained here is for Artin's billiard ($C_p = 1$). Using a method analogous to the method of images in electrostatics, the S matrix (here just a scalar since there is only one scattering channel open) can, surprisingly, be calculated explicitly. The result is [7, 11]

$$S(k) = \frac{\pi^{-\imath k}\Gamma\left(\frac{1}{2} + \imath k\right)\zeta(1 + 2\imath k)}{\pi^{\imath k}\Gamma\left(\frac{1}{2} - \imath k\right)\zeta(1 - 2\imath k)}, \tag{12}$$

where $\Gamma(z)$ is Euler's gamma function and $\zeta(z)$ is Riemann's zeta function. The resonances (poles of S) are given by the zeros of the denominator, which occur at $k = k_n/2 - \imath/4$, according to the Riemann hypothesis, where the k_n are the Riemann zeros. The 'trivial' zeros are handily cancelled by the gamma functions. The k_n are well known [8] to possess GUE level-spacing statistics. However, superimposed on this continuum are an infinite set of bound states (zero width) with Poissonian statistics due to arithmetic chaos [12]. The numerical results presented here give both the resonances on the critical line and the cusp forms in one calculation.

3. Resonance statistics

3.1. The widths

The width of a resonance is taken here to be the absolute value of its imaginary part. In atomic physics, resonances correspond to meta-stable states of a compound system, and the lifetime of a state is directly related to its width [27]. Here the widths of the eigenmomenta, not eigenenergies, are studied, since the interesting behaviour is more apparent in the momentum plane and since the two are simply related in a billiard system. Behaviour seen generically in atomic and other scattering problems is also seen here.

In random matrix models of quantum scattering, two limiting regimes can be considered; that in which the system is only 'weakly' open and resonances do not overlap much (their widths are small compared to their spacing on the real axis) and that in which there is strong coupling of the system to the continuum, where resonances may be broad and generally overlap.

The system considered here is relatively simple in that there is only one channel open for scattering (only one state which corresponds to a particle escaping to infinity). In general, in the case of weak coupling to continua, first order perturbation theory is adequate to calculate the resonance widths in terms of eigenfunctions of a suitable closed system (this can be done here by closing the billiard at some sufficiently high value of y). In this case, random matrix

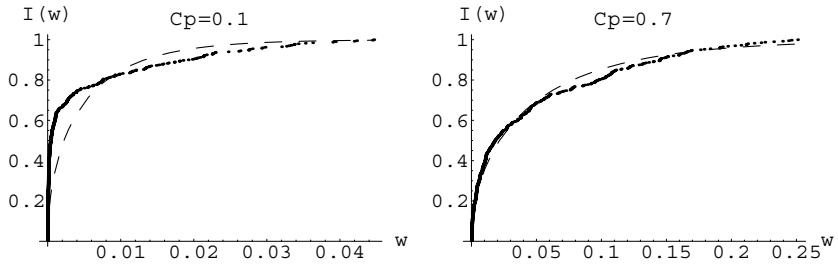

Figure 2. Integrated width density of 400 resonances for $C_p = 0.1$ and for $C_p = 0.7$. The dashed curve is the integrated Porter–Thomas distribution.

theory predicts that the width distribution for a chaotic system with M weakly open channels is given by the χ^2 distribution [28],

$$\rho(w_n) = \frac{(\nu/2)^{(\nu/2)}}{\Gamma(\nu/2)} w_n^{(\nu/2-1)} \exp\left(-\frac{\nu}{2} w_n\right), \tag{13}$$

where w_n is the resonance width normalized to its mean value, the parameter $\nu = M$ or $\nu = 2M$ for systems with time-reversal invariance or broken time-reversal invariance respectively, and $\Gamma(x)$ is Euler's gamma function again. For the system considered here, $\nu = 1$ and the corresponding distribution is known as the Porter–Thomas distribution, first derived in [29] where it provided a good fit to neutron–nuclei resonances.

Figure 2 shows the numerical integrated width density $I(w)$ for $C_p = 0.1$ and $C_p = 0.7$. The case $C_p = 0.1$ is very close to the integrable system with no resonances at all and the resonances are only just starting to move off the real axis. The dashed line is the integrated Porter–Thomas distribution

$$I(w) = \mathrm{erf}(\sqrt{w_n/2}), \tag{14}$$

where $\mathrm{erf}(x)$ is the error function, which for $C_p = 0.7$ is a reasonable fit.

Figures 3–5 show the transition to arithmetic chaos in Artin's billiard as we vary C_p near $C_p = 1$. The width distribution initially separates into two classes which at $C_p = 1$ become concentrated exactly at $w = 0$ and $w = \frac{1}{4}$. This separation is reminiscent of the so-called 'trapping phenomenon', which occurs generically when the coupling to continua exceeds some critical value. M very unstable states (broad resonances) are formed, while the remainder of the spectrum moves back to the real axis [33, 30, 31]. However, this 'spectral reorganization' usually only generates a number of broad states equal to the number of channels M which is not the case here, since $M = 1$ and an infinite set of broad states are found. As C_p is increased further the two groups merge again and the χ^2 distribution is again recovered at $C_p \approx 1.2$ (see figure 5). The phenomenon seen here is attributed purely to the arithmetic chaos at $C_p = 1$. Note that the number of resonances available is reduced as C_p increases due to the calculations being seeded at $C_p = 0$.

3.2. Level-spacing statistics

The statistics of the real parts of the resonances were also investigated. Unlike the situation for the eigenvalues of closed billiards [5], there is no formula corresponding to Weyl's law for the asymptotic density of resonance states. Instead, a numerical fit to the data is first done, to allow the 'unfolding' of the spectrum to one with unit mean level density, via the

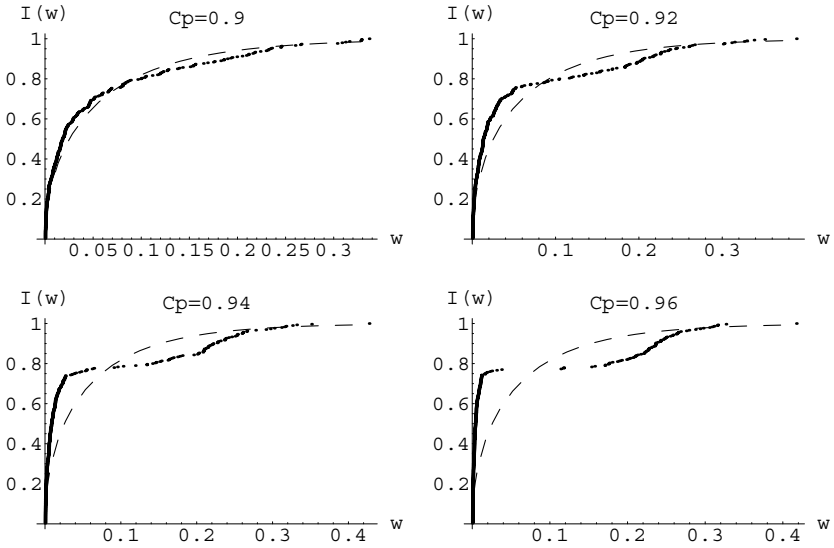

Figure 3. Integrated width densities of 300 resonances for $0.90 < C_p < 0.96$. The dashed curve is the integrated Porter–Thomas distribution.

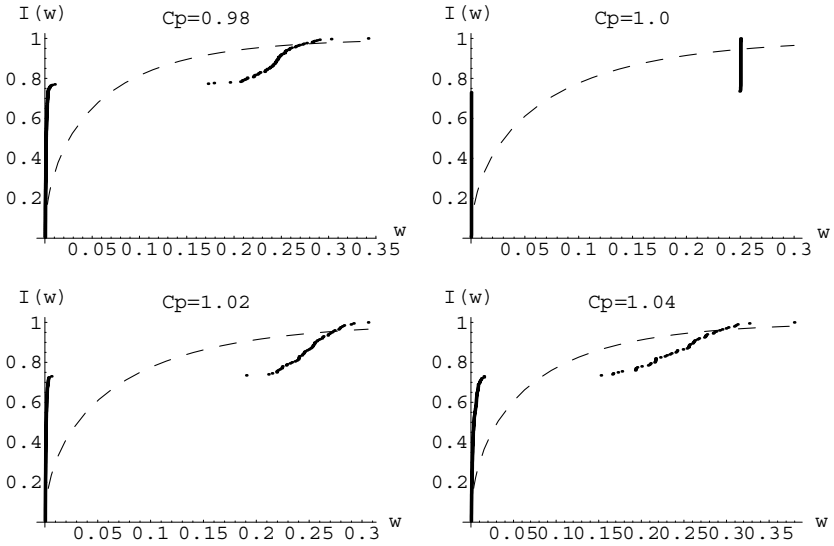

Figure 4. Integrated width densities of 200 resonances for $0.98 < C_p < 1.04$. The dashed curve is the integrated Porter–Thomas distribution.

transformation

$$x_i = \bar{N}(k_i), \tag{15}$$

where $\bar{N}(k)$ is the fitted integrated density of states for the particular billiard considered.

In terms of statistics of the unfolded eigenmomenta, the nearest-neighbour distribution is considered. The graph on the left-hand side of figure 6 shows the integrated distribution $I(s)$ of spacings between neighbouring unfolded levels ($s = x_{i+1} - x_i$) for the case $C_p = 0$,

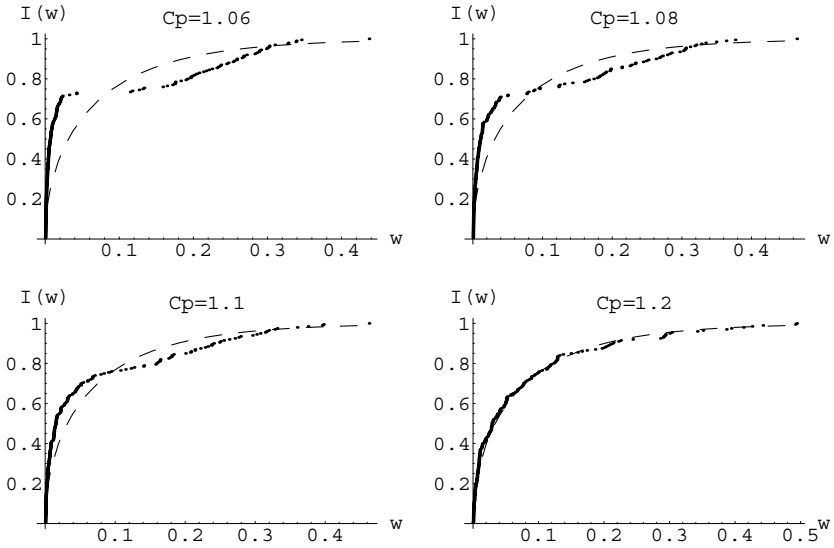

Figure 5. Integrated width densities of 200 resonances for $1.04 < C_p < 1.2$. The dashed curve is the integrated Porter–Thomas distribution.

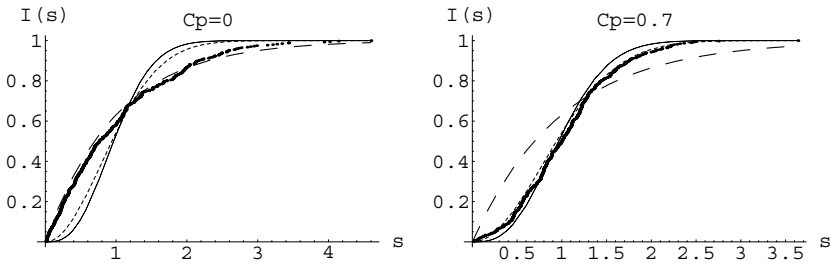

Figure 6. Integrated level-spacing distribution of 400 resonances for $C_p = 0$ and for $C_p = 0.7$. The dashed line is the integrated Poisson distribution, the finely dashed line is the GOE prediction and the solid line is the GUE prediction.

where the classical phase-space is completely integrable [21]. The distribution follows the Poissonian (dashed line) distribution

$$I(s) = 1 - \mathrm{e}^{-s}, \tag{16}$$

which is predicted for generic integrable systems [22, 23]. Also shown are the integrated Wigner surmise for both the GOE (Gaussian orthogonal ensemble) (finely dashed line)

$$I(s) = 1 - \mathrm{e}^{-\pi s^2/4}, \tag{17}$$

and the GUE (Gaussian unitary ensemble) (solid line)

$$I(s) = -\frac{4}{\pi} s\, \mathrm{e}^{-\frac{4}{\pi}s^2} + \mathrm{erf}(2s/\sqrt{\pi}), \tag{18}$$

which are very close to the distributions predicted for fully chaotic systems with time-reversal invariance and broken time-reversal invariance, respectively [24].

In the graph on the right-hand side of figure 6, the same information is shown for $C_p = 0.7$ (where the classical phase-space has become almost completely chaotic [21]). The distribution

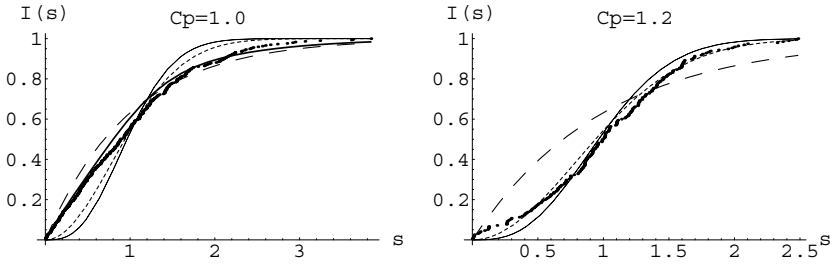

Figure 7. As figure 6 for 300 resonances at $C_p = 1$ and for 200 resonances at $C_p = 1.2$. The thick curve in the $C_p = 1$ graph is a weighted average of the integrated Poisson and GUE densities.

seems to be well described by the GOE curve. In the graph on the left-hand side of figure 7, the distribution is shown for $C_p = 1$. As expected, it does not fit any of the distributions. The group of resonances with width $\frac{1}{4}$ are known to follow GUE statistics [8] whereas the cusp forms obey the Poisson distribution. However, in the graph on the left-hand side of figure 7 a fourth curve (thick line) is plotted which is a sum of (16) and (18) weighted by the percentage of resonances from each class (approximately in the ratio 3:1 of cusps to resonances). It gives a far better fit to the data than any one of the single distributions. Finally, as C_p is increased further to $C_p \approx 1.2$, the GOE behaviour is recovered for the resonance positions (see the graph on the right-hand side of figure 7).

A method for parametrizing the variation between these distributions was proposed by Brody [25]. Although it has no sound theoretical basis such as is the case for those methods that base the parametrization on the percentage of classical phase-space which is completely chaotic, it is simple and may be applied to the situation near $C_p = 1$ where the change in statistics is due to arithmetic chaos, not a change in the classical phase-space. This is also the parametrization used in [21].

The Brody distribution, normalized to unit mean and total probability, is given by [26]

$$p(s, \nu) = a(\nu)(\nu + 1)s^{\nu} \exp(-a(\nu)s^{\nu+1}), \tag{19}$$

where

$$a(\nu) = \left(\Gamma\left(\frac{\nu + 2}{\nu + 1}\right)\right)^{\nu+1} \tag{20}$$

and $\Gamma(x)$ is Euler's gamma function. For $\nu = 0$, this gives (16) and for $\nu = 1$ (17) is obtained.

The integrated level density of the Brody distribution is

$$I(s, \nu) = \int_0^s p(x, \nu)\,\mathrm{d}x = 1 - \exp(-a(\nu)s^{\nu+1}). \tag{21}$$

Brody distributions were fitted to the numerical integrated density functions obtained (the error on the fit is much lower than for fitting to the density itself), using the method of least squares. The calculated values of ν give a useful measure of how close the distribution is to (16) or (17). Figure 8 shows the variation of the derived ν with C_p in the range $0 \leqslant C_p \leqslant 1.2$. A similar result was obtained by Csordás *et al* in [21], for the bound states for billiards with Dirichlet boundary conditions. The distribution moves from Poissonian in the case where the classical dynamics are fully integrable up to GOE when they are completely chaotic. The sharp transition to near-Poissonian statistics at $C_p = 1$, in the sense that there are many more cusp forms than resonances with width $\frac{1}{4}$ in a given energy range, is shown in more detail. The value of ν obtained here for $C_p = 1$ agrees well with the scaling behaviour with N, the

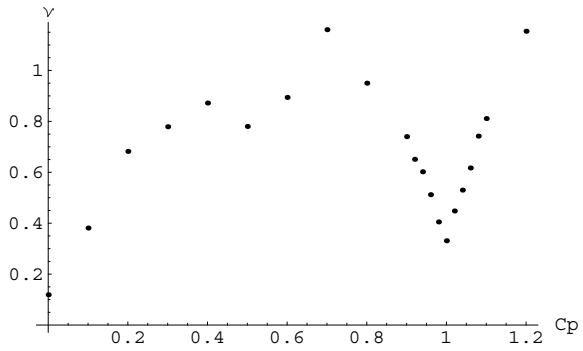

Figure 8. Variation of the Brody parameter ν with C_p.

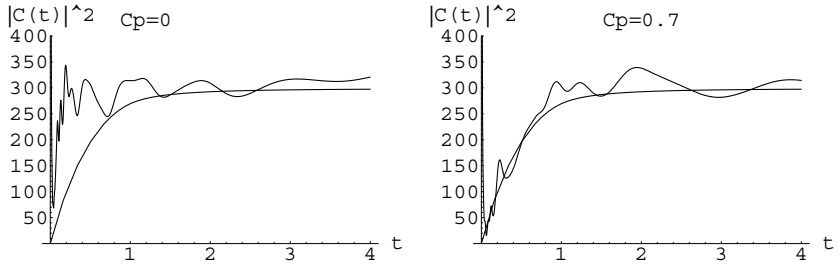

Figure 9. Gaussian smoothed absolute square of the Fourier transform of the spectrum at $C_p = 0$ and for $C_p = 0.7$. The smooth line is the GOE prediction.

number of eigenvalues found, which was seen in [21]. The transition to arithmetic chaos at $C_p = 1$ is clearly defined.

3.3. Fourier transform of the spectra

To check on higher order correlation functions, e.g. two-point correlations, and to compare further with RMT predictions the Fourier transform of the positions of the resonances have been calculated [32]. Figure 9 shows the modulus squared of the direct Fourier transform,

$$C(t) = \int_{-\infty}^{\infty} \sum_{i=1}^{N} \delta(k_i - k)\, \mathrm{e}^{-2\pi\imath kt}\, \mathrm{d}k, \tag{22}$$

of the real parts of the resonance positions for the values of C_p shown, after a Gaussian smoothing has been applied with width $\sigma = t/10$, following Alt *et al* [34] who give a recent review of the method in the context of superconducting microwave billiards. In addition, the ensemble averaged curve predicted by RMT for the GOE is plotted.

$$|C(t)_{GOE}|^2 = |b(t) - 1|^2, \tag{23}$$

where

$$b(t) = \begin{cases} 1 - 2t + t\ln(1+2t) & 0 < t < 1 \\ -1 + t\ln((2t+1)/(2t-1)) & t > 1. \end{cases}$$

The Fourier transforms were performed on 300 levels. The correlation hole predicted by RMT for GOE systems for small t is present in the case $C_p = 0.7$ and is filled for $C_p = 0$,

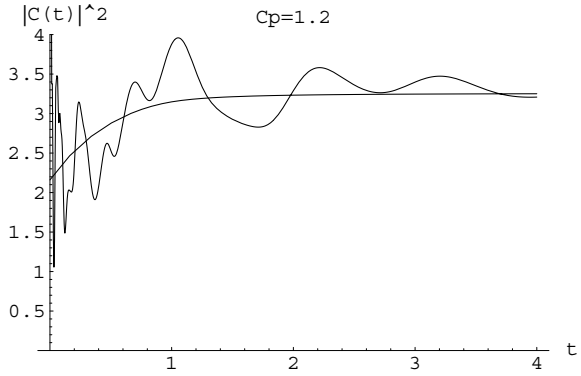

Figure 10. Gaussian smoothed absolute square of the Fourier transform of the width-weighted spectrum at $C_p = 1.2$. The smooth line is the GOE prediction.

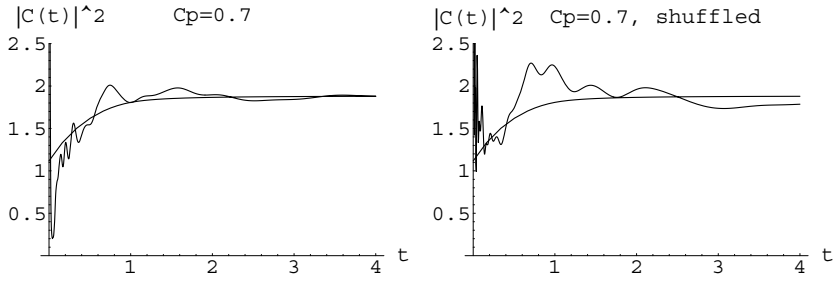

Figure 11. Gaussian smoothed absolute square of the Fourier transform of the width-weighted spectrum at $C_p = 0.7$ (left) and the same for the widths distributed randomly rather than on their corresponding positions (right). The smooth line is the GOE prediction.

consistent with RMT predictions for a system obeying Poissonian statistics. In the case $C_p = 1$, it is well known that the Fourier transform for the spectrum defined by the Riemann zeros follows the GUE prediction remarkably closely [8]. The same behaviour is seen in the Fourier transform for $C_p = 1.2$ as for $C_p = 0.7$.

3.4. Correlations between widths and positions

It is also of interest in scattering systems to examine if there is any correlation between the positions and widths of the resonances. RMT predicts that there should be no correlation for weakly open systems with isolated resonances. This can be tested for, again using Fourier transforms, but now applied to a spectrum weighted by the widths [35]:

$$C(t) = \int_{-\infty}^{\infty} \sum_{i=1}^{N} w_i \delta(k_i - k)\, \mathrm{e}^{-2\pi \imath k t}\, \mathrm{d}k. \tag{24}$$

The prediction of random matrix theory for the GOE case is that the correlation hole is filled by two-thirds [35], as is seen in figure 10 for $C_p = 1.2$.

However for $C_p = 0.7$, as seen on the left-hand side of figure 11, there is a dip in the Fourier transform for very short times which is at odds with RMT predictions even though the widths are well described by the Porter–Thomas distribution and the resonance positions

by GOE and the RMT two-point correlation function. The graph on the right-hand side of figure 11 demonstrates that the correlations are destroyed if the widths are assigned randomly to positions. This indicates the existence of long-range non-universal correlation between the positions and widths. A similar correlation between positions and intensities was found in a study of chaotic Rydberg molecules [35]. The origin of the above correlations will be investigated in future work.

4. Conclusions

A class of open billiards on the Poincaré half-plane parametrized by the inverse-radius of the lower boundary was investigated. The resonance positions were determined as a function of this parameter. The classical dynamics of these billiards varies from integrable to fully chaotic and good agreement was found with the predictions of random matrix theory for the distributions of both the spacings of the real parts of the resonant momenta, and for the absolute values of the imaginary parts. As variation in the parameter brings the system closer to Artin's billiard, the resonances divide quickly into two classes. The first is those resonances with width $\frac{1}{4}$, which possess GUE level-spacing statistics, and the second is those resonances which move back to the real axis where they form bound states with Poissonian level-spacing statistics. This transition was investigated more closely and a Brody parameter was found to give a good fit of the variation of the distributions. Increasing the parameter further, the resonances redistribute themselves and the two groups merge once again to form distributions consistent with random matrix theory. In certain parameter ranges, non-universal long-range correlations were seen in the Fourier transform of the width-weighted spectrum indicating correlations between the resonance positions and widths. These correlations will be investigated in future work.

Acknowledgments

The authors wish to thank Holger Then for the use of his routines for calculating the K-Bessel functions. PJH is supported by an EPSRC postgraduate studentship.

References

[1] Bohigas O, Gianonni M J and Schmit C 1984 *Phys. Rev. Lett.* **54** 1
[2] Haake F 1992 *Quantum Signatures of Chaos* 2nd edn (Berlin: Springer) p 47
[3] Balázs B V and Voros A 1986 *Phys. Rep.* **143** 109
[4] Bogomolny E B, Georgeot B, Giannoni M-J and Schmit C 1992 *Phys. Rep.* **291** 219
[5] Csordás A, Graham R and Szépfalusy P 1991 *Phys. Rev.* A **44** 1491
[6] Aurich R, Lustig S, Steiner F and Then H 2005 *Phys. Rev. Lett.* **94** 021301
[7] Gutzwiller M C 1990 *Chaos in Classical and Quantum Mechanics* (Berlin: Springer) p 376
[8] Odlyzko A M 1989 The 10^{20}th zero of the Riemann zeta function and 70 million of its neighbours *Preprint* AT&T Bell Laboratories
[9] Odlyzko A M *The first 100,000 zeros of the Riemann zeta function, accurate to within* $3 * 10^{-9}$ http://www.dtc.umn.edu/odlyzko/zeta_tables/zeros1
[10] Friedrich H 1998 *Theoretical Atomic Physics* (Berlin: Springer) p 145
[11] Wardlaw D M and Jaworski W 1989 *J. Phys. A: Math. Gen.* **22** 3561
[12] Bolte J, Steil G and Steiner F 1992 *Phys. Rev. Lett.* **69** 2188
[13] Schmit C 1989 *Chaos et Physique Quantique—Chaos and Quantum Physics, Les Houches, ecole d'éte de physique theorique 1989, session LII* ed M Giannoni *et al* (Amsterdam: Elsevier)
[14] Backer A 2002 Numerical aspects of eigenvalue and eigenfunction computations for chaotic quantum systems *Preprint* nlin.CD/0204061

[15] Anderson E *et al* 1999 *LAPACK Users' Guide* 3rd edn (Philadelphia, PA: SIAM)
[16] Steil G 1994 Eigenvalues of the Laplacian and of the Hecke operators for **PSL**$(2, \mathbb{Z})$ *DESY report* 28-94, Hamburg
[17] Hejhal D A and Berg B 1982 Some new results concerning eigenvalues of the non-Euclidean Laplacian for **PSL**$(2, \mathbb{Z})$ *Technical Report* 82-172, University of Minnesota
[18] Wolfram Research, Inc. 2004 *Mathematica, Version 5.1* (Champaign, IL: Wolfram Research, Inc.)
[19] Abramowitz M and Stegun I A 1965 *Handbook of Mathematical Functions* (New York: Dover)
[20] Then H 2005 *Math. Comp.* **74** 363
[21] Csordás A, Graham R, Szépfalusy P and Vattay G 1994 *Phys. Rev.* E **49** 325
[22] Berry M V and Tabor M 1977 *Proc. R. Soc. Lond.* A **356** 375
[23] Robnik M and Veble G 1998 *J. Phys. A: Math. Gen.* **31** 4669
[24] Stöckmann H-J 1999 *Quantum Chaos: An Introduction* (Cambridge: Cambridge University Press) p 87
[25] Brody T A 1973 *Lett. Nuovo Cimento* **7** 482
[26] Stöckmann H-J 1999 *Quantum Chaos: An Introduction* (Cambridge: Cambridge University Press) p 94
[27] Taylor J 1972 *Scattering Theory* (New York: Wiley) p 238
[28] Fyodorov Y V and Sommers H-J 1997 *J. Math. Phys.* **38** 1918
[29] Porter C E and Thomas R G 1956 *Phys. Rev.* **104** 483
[30] Persson E, Rotter I, Stöckmann H-J and Barth M 2000 *Phys. Rev. Lett.* **85** 2478
[31] Haake F, Izrailev F, Lehmann N, Saher D and Sommers H-J 1992 *Z. Phys.* B **88** 359
[32] Leviandier L, Lombardi M, Jost R and Pique J P 1986 *Phys. Rev. Lett.* **56** 2449
[33] Sokolov V V and Zelevinsky V G 1988 *Nucl. Phys.* A **504** 562
[34] Alt H, Gräf H-D, Guhr T, Harney H L, Hofferbert R, Rehfeld H, Richter A and Schardt P 1997 *Phys. Rev.* E **55** 6674
[35] Lombardi M and Seligman T H 1993 *Phys. Rev.* A **47** 3571